Nuclear Fusion

PAPER

Control of the hydrogen:deuterium isotope mixture using pellets in JET

To cite this article: M. Valovi *et al* 2019 *Nucl. Fusion* **59** 106047

IOP Publishing | International Atomic Energy Agency Nuclear Fusion

Nucl. Fusion **59** (2019) 106047 (7pp) https://doi.org/10.1088/1741-4326/ab3812

Control of the hydrogen:deuterium isotope mixture using pellets in JET

M. Valovič[1], Y. Baranov[1], A. Boboc[1], J. Buchanan[1], J. Citrin[2], E. Delabie[3], L. Frassinetti[4], J.M. Fontdecaba[5], L. Garzotti[1], C. Giroud[1], R. McKean[1], E. Lerche[1,6], V. Kiptily[1], F. Köchl[1,7], M. Marin[2], M. Maslov[1], S. Menmuir[1], G. Tvalashvili[1], H. Weisen[1] and the JET Contributors[a]

EUROfusion Consortium, JET, Culham Science Centre, Abingdon OX14 3DB, United Kingdom of Great Britain and Northern Ireland

[1] CCFE, Culham Science Centre, Abingdon OX14 3DB, United Kingdom of Great Britain and Northern Ireland

[2] DIFFER, PO Box 6336, 5600 HH Eindhoven, Netherlands

[3] Oak Ridge National Laboratory, Oak Ridge, TN, United States of America

[4] KTH Royal Institute of Technology, TEKNIKRINGEN 31, Sweden

[5] Laboratorio Nacional de Fusión, Ciemat, 28040 Madrid, Spain

[6] LPP-ERM/KMS, Association EUROFUSION-Belgian State, TEC Partner, Brussels, Belgium

[7] Fusion@ÖAW, Atominstitut, TU Wien, Stadionallee 2, A-1020 Vienna, Austria

E-mail: martin.valovic@ukaea.uk

Received 18 March 2019, revised 9 July 2019
Accepted for publication 2 August 2019
Published 9 September 2019

Abstract

Deuterium pellets are injected into an initially pure hydrogen H-mode plasma in order to control the hydrogen:deuterium (H:D) isotope mixture. The pellets are deposited in the outer 20% of the minor radius, similar to that expected in ITER, creating transiently hollow electron density profiles. A H:D isotope mixture of approximately 45%:55% is obtained in the core with a pellet fuelling throughput of $\Phi_{\mathrm{pel}} = 0.045 P_{\mathrm{aux}}/T_{\mathrm{e,ped}}$ similar to previous pellet fuelling experiments in pure deuterium. Evolution of the H:D mix in the core is reproduced using a simple model, although deuterium transport could be higher at the beginning of the pellet train compared with the flat-top phase.

Keywords: tokamak, isotope mix control, pellet fuelling

(Some figures may appear in colour only in the online journal)

1. Introduction

To maximize the power produced by a fusion reactor the deuterium:tritium (D:T) isotope mixture should be kept close to 50%:50%. This can be achieved simply by fuelling the reactor with pre-mixed DT fuel. Such a fuelling scheme would avoid isotope separation in the reactor's outer fuel loop and only requires hydrogen isotopes to be separated from helium and impurities. Avoidance of isotope separation will reduce the cost of the reactor, but more importantly it will decrease the dwell time of tritium in the outer loop and reduce the amount of tritium in the reactor.

Complete removal of isotope separation from the fuel loop, however, could make control of the isotope mix impossible. The D:T ratio in the plasma core can gradually drift from its pre-mixed value, for a number of reasons. Firstly, it has been widely observed in tokamak plasmas that different hydrogenic isotopes have moderately to significantly differing energy and particle confinement parameters, with transport typically reducing at higher isotope mass. Gyro-kinetic analysis and modelling have identified mechanisms for this differentiation of the tokamak particle transport coefficient between hydrogenic isotopes [1–4], although in practice the resultant density profile separation is expected to be weak. However, the isotope dependence of pedestal transport is more uncertain. Secondly, for engineering reasons, neutral beams are likely to inject pure deuterium as planned on ITER.

[a] See the author list of Joffrin *et al* [28].

Although the fuelling efficiency of neutral beams is low it is still comparable to the fusion rate, and thus beams could lead to an excess of deuterium in the plasma core. It could be mentioned here, however, that in ion temperature gradient (ITG) regimes the sensitivity of isotope peaking to the isotope source is expected to be weak [4, 5] and depends more on core isotope boundary conditions and electron density peaking. Finally, departure from a 50%:50% isotope mix can arise from different particle exhaust and wall recycling for deuterium and tritium, affecting the core boundary conditions. Due to all these uncertainties ITER is planning full isotope separation and two sets of pellet injectors, one for pure tritium and one for pure deuterium [6, 7]. In DEMO a compromise solution with partial separation (bypass) is considered [8].

The requirement for accuracy of control of the isotope mix itself is not very demanding. At fixed electron density, ignoring helium and impurities, keeping fusion power within say 5% of its maximum value requires a D:T density ratio within $n_T/(n_D + n_T) = 0.4$–0.6. The main uncertainty is the time scale over which the isotope ratio should be controlled in this window and what throughput of pure tritium is required to achieve that.

This question cannot be answered directly even on JET as the pellet injector is not designed to operate in tritium. Nevertheless, pellet fuelling experiments can be designed in JET which partially address the aforementioned problem. Firstly, deuterium pellets could be injected into plasma which has been pre-fuelled by tritium gas and beams, and such an experiment is proposed for the next DT campaign in JET. Another possibility of how to contribute is to inject combinations of hydrogen and deuterium pellets and observe and understand different isotope behaviours. The present paper describes one such experiment in which pure deuterium pellets were injected into hydrogen plasma and successfully maintained the H:D isotope mix close to the 50%:50% target. We note that isotope control using pre-mixed HD pellets was performed on ASDEX Upgrade [9] including very detailed documentations of the preparation and diagnostics of mixed isotope pellets. Finally note that isotope experiments using pellets are rare but there is a considerable body of data on isotope dependences using gas and beams from previous experiments on TFTR [10, 11], JT-60U [12] and JET [13] as well as recent data from JET and ASDEX Upgrade [14].

2. Experimental setup

The experiment was performed on JET with ITER-like walls with a plasma current $I_p = 1.4$ MA and a toroidal field on geometric axis $B_T = 1.7$ T. The divertor was in the corner configuration for both the inner and outer legs. Plasma fuelling was provided by hydrogen gas with a rate of $\Phi_{H_2,gas} = 6.7 \times 10^{21}$ atoms/s, which was reduced to 5.2×10^{21} atoms/s during the pellet phase (see figure 1(*c*)).

The plasma was heated by hydrogen neutral beams with total flat-top power of $P_{NBI} = 6.3$ MW. The corresponding particle source from the beams is $\Phi_{H2,NBI} = 1.5 \times 10^{21}$ atoms/s. In addition, RF heating at the second harmonic hydrogen resonance ($\omega = 2\omega_{cH}$, 51 MHz) is used with total power of $P_{RF} = 3.3$ MW so that the total auxiliary heating power during flat-top is $P_{aux} = 9.6$ MW.

After a stationary hydrogen H-mode has been established, additional fuelling by deuterium pellets from the high-field side is applied. (The choice of high-field side launching is to mimic the ITER situation which takes advantage of the magnetic drift effect and results in deeper pellet deposition compared with low-field side injection.) As seen in figure 1(*b*) each pellet causes a sharp increase in the line-integrated plasma density. The nominal pellet volume given by the extruder is 40 mm^3. Using the 'double-cut' technique (which changes the circular pellet cross-section to a 'moon-like' cross-section) we reduced the pellet volume by approximately a factor of two to get closer to the ITER situation: the volume of fuelling pellets in ITER is 90 mm^3 [7], which scaled by plasma volume corresponds to 11 mm^3 in JET, about half being 'double-cut' pellets. Pellet size is variable when using the double-cut technique, as seen in figure 1, because of higher sensitivity of pellet shape to the extrusion rate compared with conventional injector operation. Pellets are applied in feed-forward mode. Before pellets are injected into the plasma their frequency and size are measured in a microwave cavity utilizing the change of resonance in the presence of the pellet. The averaged values over the interval $t = 12.2$–15.0 s are $f_{pel} = 9.7$ Hz for pellet frequency and $N_{pel} = 8.5 \times 10^{20}$ atoms for pellet particle content, so that the pellet fuelling rate is $\Phi_{pel} = 8.2 \times 10^{21}$ atoms/s. The pellet velocity is ~ 90 m s^{-1}.

3. Measurement of the isotope mix ratio

During injection of deuterium pellets into hydrogen plasma the isotope mix ratio was measured by four independent methods as listed below.

3.1. From neutrals by Balmer-alpha and Penning gauges

Figure 1(*a*) shows the ratio $n_D/(n_H + n_D)$ as measured by Balmer-alpha spectroscopy in the divertor and in the Penning gauges in the subdivertor. The values agree well, which is not surprising as both methods measure the isotope mix ratio of neutrals in the divertor region. It can be also observed that both ratios need about 2 s to reach the flat-top value of

$$n_D/(n_H + n_D)_{\text{edge neutrals}} \approx 0.35.$$

3.2. From CX

Information about the isotope ratio of ions in the plasma core can be obtained using charge exchange (CX) spectroscopy. This system is different from that described in section 3.1. Two Gaussian functions are fitted to the hydrogen and deuterium Balmer-alpha CX lines assuming the same temperature and rotation for both isotopes. The key element of the analysis is to achieve very good subtraction of passive background light. We have employed modulation of the neutral beam used for CX spectroscopy and remove all frames of data with

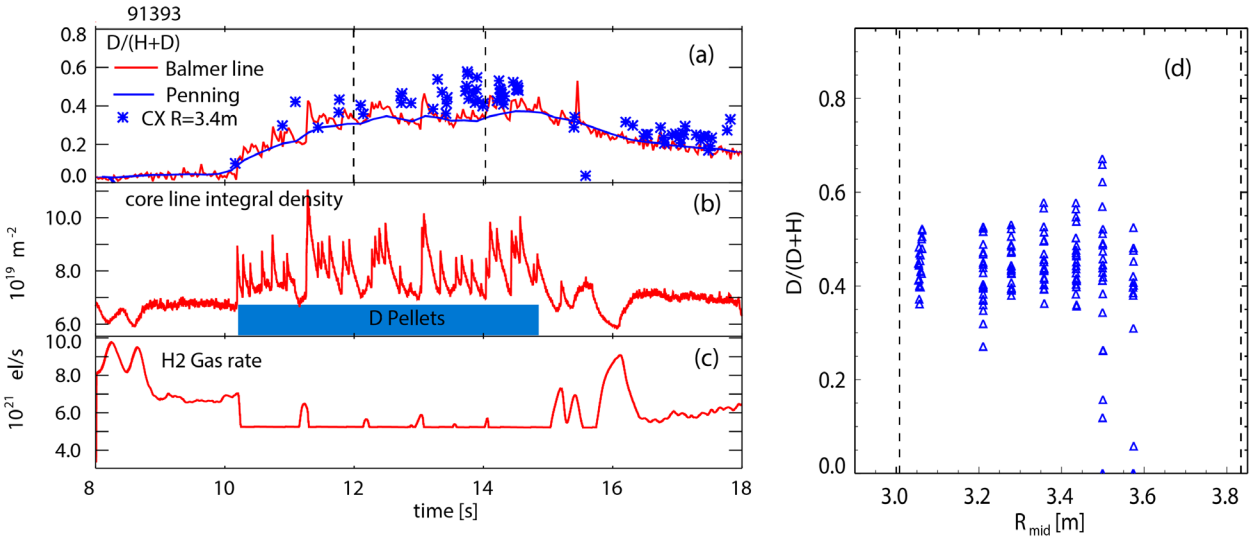

Figure 1. Temporal evolution of relevant parameters during the isotope control experiment. Traces from the top to the bottom: (*a*) isotope mix ratio from Balmer line spectroscopy (red line), Penning pressure gauges in the divertor (blue line), charge exchange (CX) spectroscopy at $R = 3.43$ m (normalized minor radius $r/a = 0.27$) (blue symbols); (*b*) core line integrated density n_eL; (*c*) hydrogen gas puff rate. (*d*) Isotope mix ratio profile from CX spectroscopy for the time interval shown by vertical lines in panel (*a*). The vertical lines in panel (*d*) represent the magnetic axis and separatrix, respectively. For a given radius different data points represent different times.

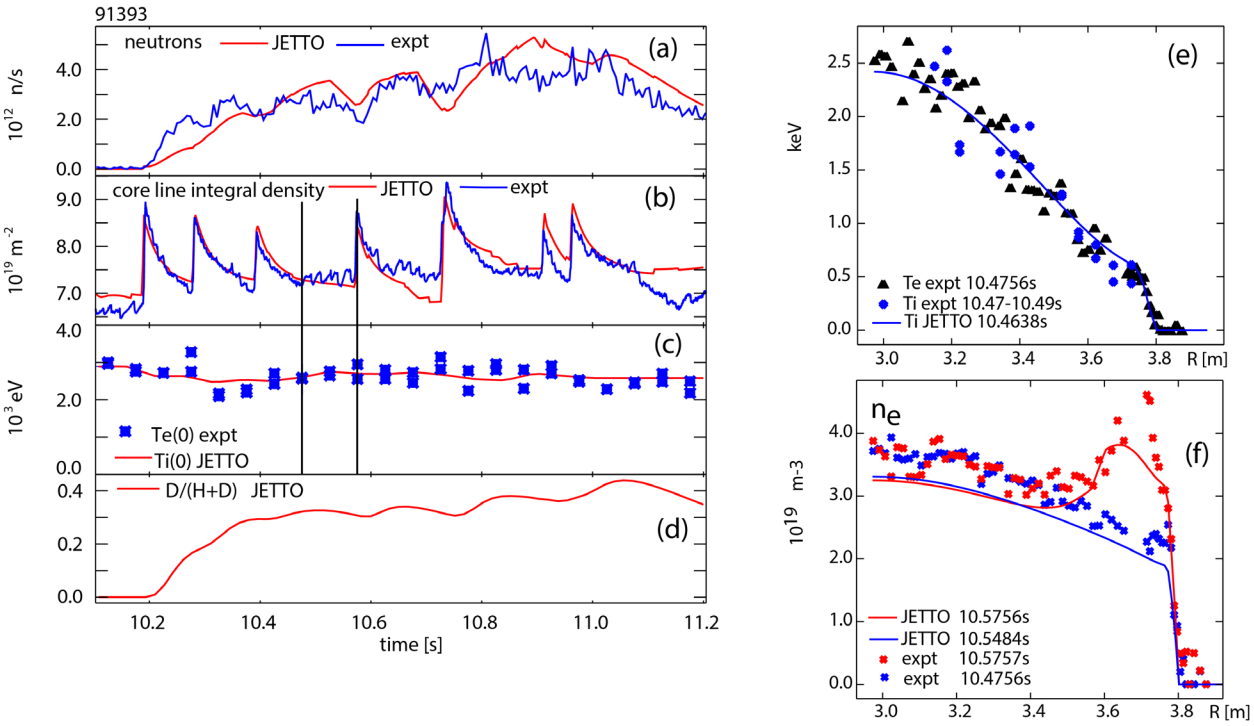

Figure 2. Simulation of isotope mix by the JETTO code. (*a*) Total neutron rate $R_{DD,th}$. (*b*) Core line integrated density n_eL with error bar of 5×10^{17} m^{-2}. (*c*) Central electron temperature from Thomson scattering (blue symbols) and central ion temperature as imported into JETTO (red line). (*d*) Calculated central isotope mix ratio $n_D/(n_H + n_D)$ from the neutron rate. (*e*) Electron and ion temperatures and (*f*) electron density profiles before and after the fourth pellet (for timing see the vertical bars in panels (*b*) and (*c*)). In panels (*e*) and (*f*) electron density and temperature are measured by Thomson scattering.

edge-localized mode (ELM) crashes or pellet injection due to strong variation in the background light. Details of these diagnostics will be published elsewhere. In our case the isotope mix ratio can be evaluated well inside the plasma with some limitation close to the magnetic axis and outer part of the plasma where error bars become very large. The CX method gives the flat-top value of (figures 1(*a*) and (*d*))

$$n_{\mathrm{D}}/(n_{\mathrm{H}}+n_{\mathrm{D}})_{R=3.1\text{–}3.4\,\mathrm{m}} \approx 0.45.$$

This core value is somewhat higher than the neutral gas measurements from the edge plasma.

3.3. From neutrons

The isotope mix ratio can be deduced indirectly from the neutron rate. Figure 2(*a*) shows that application of deuterium pellets causes an increase in the neutron rate from virtually zero to the flat-top value of $R_{\mathrm{n}} = (3\text{–}4) \times 10^{12}$ neutrons/s, confirming that the deuterium from pellets penetrated into the plasma core and produced DD fusion reactions. Assuming that all neutrons are the result of a thermal DD reaction, and knowing the density and temperature profiles, one can convert the neutron rate into the isotope mix ratio in the centre. The problem is the discrete nature of pellet fuelling which makes the plasma density transient at all times. To include this element into the analysis, we calculated the plasma density using a model while keeping the temperature fixed from the measurement. The model evolves hydrogen and deuterium densities independently as a response to particle sources and particle transport. In other words temperature is treated interpretatively while densities are treated predictively. The simulation was done by JINTRAC code suite [15]. The particle sources include beams, pellets and neutrals, and are calculated by PENCIL, HPI2 and FRANTIC codes, respectively. The boundary condition for FRANTIC is set by a neutral hydrogen flux of Φ_0 at the separatrix.

The particle transport is modelled by the JETTO code. For the plasma core the particle diffusivity is $D = C_{\mathrm{D}} \times \chi_{\mathrm{BgB}}$, where χ_{BgB} is the geometric average of the electron and ion Bohm/gyro-Bohm heat diffusivities [15, 16] and the C_{D} multiplier is set to be the same for hydrogen and deuterium. A modest inward anomalous pinch is also included, as $v/D = -C_{\mathrm{V}} r/a^2$. The motivation for core particle transport modelling was to infer the particle transport coefficients D and V, leading to experimental agreement for later comparison with higher-fidelity first-principle-based modelling. At the plasma edge the particle transport is modelled by the 'continuous ELM model' [17] in which the particle diffusivity inside the edge transport barrier is enhanced when the pressure gradient exceeds the critical value of $\alpha > \alpha_{\mathrm{crit}}$. Comparison of the simulation of edge density with experimental data reveals that the aforementioned ELM model does not fully describe the post pellet ELM loss mechanism. Namely, ELMs remove pellet material faster than in the model and they also act more deeply than the edge transport barrier. To include this we added transient post-pellet outward convection in the form of $v = v_0 \times \exp\left[-\left(t - t_{\mathrm{pel}}\right)/\tau + \left(r/a - 1\right)/\Delta\right]$ where v_0 is the amplitude of outward convection, τ is the duration of the enhanced post-pellet convection and Δ is the normalized radial depth of the zone of the enhanced convection. Note that the need to extend the radial extent of ELM-related particle losses more deeply than the pedestal width has been recognized in previous simulations [18].

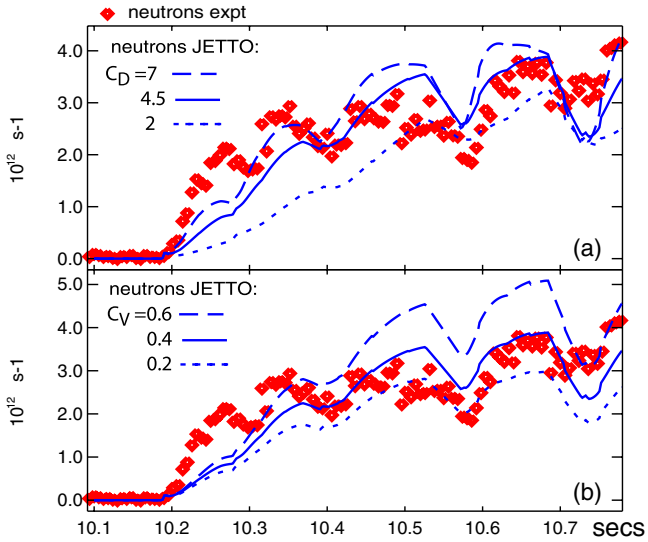

Figure 3. Comparison of measured and simulated neutron rates during the scan of particle transport coefficients: (*a*) diffusivity scan with $C_{\mathrm{D}} = 2$, 4, 5 and 7 at $C_{\mathrm{V}} = 0.4$ and (*b*) pinch velocity scan with $C_{\mathrm{V}} = 0.2$, 0.4 and 0.6 at $C_{\mathrm{D}} = 4.5$.

Figure 2 shows the result of the simulation with the following parameters $\Phi_0 = 2.7 \times 10^{21}$ atoms/s, $C_{\mathrm{D}} = 4.5$, $C_{\mathrm{V}} = 0.4$, $v_0 = 7\,\mathrm{m\,s^{-1}}$, $\tau = 50$ ms and $\Delta = 0.25$, and using the same values for hydrogen and deuterium. All these parameters are derived iteratively from the fit to experimental data as it is described below. The calculation is performed in a limited time interval starting just before the first pellet and finishing after the seventh pellet, i.e. when the neutron rate approximately reaches its maximum value.

Figures 2(*c*), (*e*) and (*f*) document how the experimental ion temperature was imported into the simulation, in particular its central value to which the thermal DD fusion rate is very sensitive. The central ion temperature from carbon and neon CX is measured with coarse time resolution and with a larger error bar. Nevertheless, in our plasma the electron and ion temperature are similar with good accuracy, as seen in panel 2(*e*), and we assume $T_{\mathrm{i}} = T_{\mathrm{e}}$. In addition, figure 2(*c*) shows that the central electron temperature is quite constant in time without transients which would otherwise introduce large variation of the neutron rate.

Figures 2(*b*) and (*f*) compare measured and calculated electron density. It is seen that the simulations reproduce well the temporal evolution of line-integrated electron density, including pellet-induced transients. The comparison of density profiles across the fourth pellet (figure 2(*f*)) also shows that density peaking just before the pellet is well captured by the simulation. The model also describes the pellet deposition depth as calculated by the HPI2 module [19] and confirms the shallow pellet deposition, similar to that expected in ITER. The simulation sometimes underestimates the amplitude of the pellet density perturbation. This is a result of the continuous

ELM model which already starts to remove the pellet particles during the pellet deposition phase. This is in contrast to an experiment where pellet particles are removed in discrete steps during the ELMs, as described in the next section.

Figure 2(*a*) compares the measured neutron rate with that calculated by the JETTO code. The neutron rate was also checked with TRANSP [20] and good agreement with JETTO was found. The agreement between the measured neutron rate and that calculated by JETTO is rather good, taking into account the large sensitivity of the thermal DD reaction rate to ion temperature. The simulation also describes well the transient responses of neutron rate on individual pellets during the flat-top phase. The sensitivity of the calculated neutron rate to a selection of transport parameters is illustrated in scans shown in figure 3. It is seen that the experimental neutron rate can be broadly bracketed by simulations using diffusivity parameters $C_D = 2$–7 and $C_V = 0.2$–0.6. The wide range of these parameters does not mean that they represent the uncertainty in the fit. They rather reflect the fact that these parameters vary in time while in our simulations they are constant. This is clearly seen in figure 3 by comparing the neutron rate during first and fourth pellets (at 10.2 s and 10.6 s, respectively). At the fourth pellet the choice $C_D = 4.5$ and $C_V = 0.4$ fits well with the neutron rate, while the same setting at the first pellet systematically underestimates the measured neutron rate.

We do not have full explanation for this discrepancy. One possibility is the isotope dependence of particle diffusivity. During the first pellet, plasma is still predominantly composed of hydrogen, while during the fourth pellet about one-third of ions are deuterium so that the effective ion diffusivity could be higher at the beginning of pellet train compared with later phases. Indeed this can be effectively introduced in the model by the time-dependent multipliers C_D and C_V. However, the discrepancy in the early neutron rate could be also related to the recent observation of anomalously fast propagation of the isotope mix ratio. This effect is recalled below at the end of section 4.2 and its investigation under our conditions will be the subject of a dedicated paper.

Another possible explanation for the increase in neutron rate could be a non-Maxwellian distribution of deuterium ions. Indeed, inspection of neutral particle analyser spectra shows an increase of deuteron fluxes for energies of 300 kV to 800 keV with an e-folding energy scale of 123 keV. This increase correlates with the timing of the pellet train. There are two possibilities for how deuterons can be accelerated to such high energies, and both are related to RF heating which is continuously applied before and during the pellet train. The first possible acceleration channel is the parasitic four-harmonic resonance $\omega = 4\omega_{cD}$. To test this we ran a shot JPN 91238 with modulated RF heating and found that the changes in neutron rate were fully in line with changes in electron temperature and parasitic resonance was not required to explain the neutron rate (note that this shot had deuterium beams so the neutron rate was due to beam–thermal interaction). The second possibility for how to accelerate deuterons to the aforementioned energies is elastic nuclear collisions between RF accelerated hydrogen ions and cold deuterium ions, the so-called knock-on effect. Order of magnitude estimates indicate that such a mechanism could produce a neutron rate comparable to the thermal–thermal levels [21]. We do not have tools to evaluate the precise contribution of knock-on to the calculated neutron rate, and consequently the isotope mix ratio. We speculate that if the knock-on effect is relevant it is probably during the beginning of pellet train where the discrepancy between modelled and measured neutron rates is largest. In support of this, CX measurement during the flat top phase (figure 1(*d*)) does not show significant reduction of the deuterium density towards the plasma core that would be required to accommodate non-thermal neutrons.

In summary, assuming that all neutrons are due to thermal DD reactions then the isotope mix ratio, as calculated by the JINTRAC code, is shown in figure 2(*d*). It is seen that at the time of maximum neutron rate (~11 s) the ratio is:

$$n_D/(n_H + n_D)_{r=0,\text{neutrons}} \approx 0.44.$$

This value is close to the CX measurement and close to the target value of 0.5.

4. Fuelling efficiency

The efficiency of isotope mix control depends on two mechanisms: (1) the amount of pellet particle flux required to keep the plasma density and isotope mix at the plasma edge at the prescribed value and (2) the characteristic time of propagation of the isotope mix from the pellet deposition zone to the plasma core. These two processes contribute multiplicatively to the pellet fuelling efficiency, i.e. good efficiency requires simultaneously a long enough lifetime of pellet density perturbation and fast enough particle transport in the core. The next sections quantify these two factors separately.

4.1. Pellet particle flux

As shown in previous sections, a deuterium pellet particle flux of $\Phi_{pel} = 8.2 \times 10^{21}$ atoms/s is sufficient to keep the isotope mix ratio at $n_D/(n_H + n_D) = 0.45$ during flat-top. (The pellet-related particle confinement time is $N_e/\Phi_{pel} \sim 0.24$ s where $N_e \sim 2.0 \times 10^{21}$ is the number of electrons in the plasma.) During the same time interval the averaged pedestal electron temperature is $T_{e,ped} = 0.33 \pm 0.05$ keV which gives a pellet fuelling flux of $\Phi_{pel} = 0.045\, P_{aux}/T_{e,ped}$. The reason why the pellet particle fuelling throughput is expected to be a fixed factor of $P_{aux}/T_{e,ped}$ is that in our experiments pellet fuelling dominates the particle flux at the pedestal and convective ELMs represent a significant fraction of particle and energy loss. For more details on this value in our experiments see [22, 23] and for ITER assumptions see [7].

To compare our value of Φ_{pel} with the case of deuterium pellets and deuterium plasma we can write $\Phi_{pel,D\to D} = \Phi_{pel} \times (n_H + n_D)/n_D$ which gives:

$$\Phi_{pel,D\to D} = 0.10 P_{aux}/T_{e,ped}. \quad (1)$$

The coefficient on the RHS of equation (1) is higher by a factor of 1.4–2 than that found in our previous pellet fuelling experiments in pure deuterium plasmas [23]. Although the dataset is

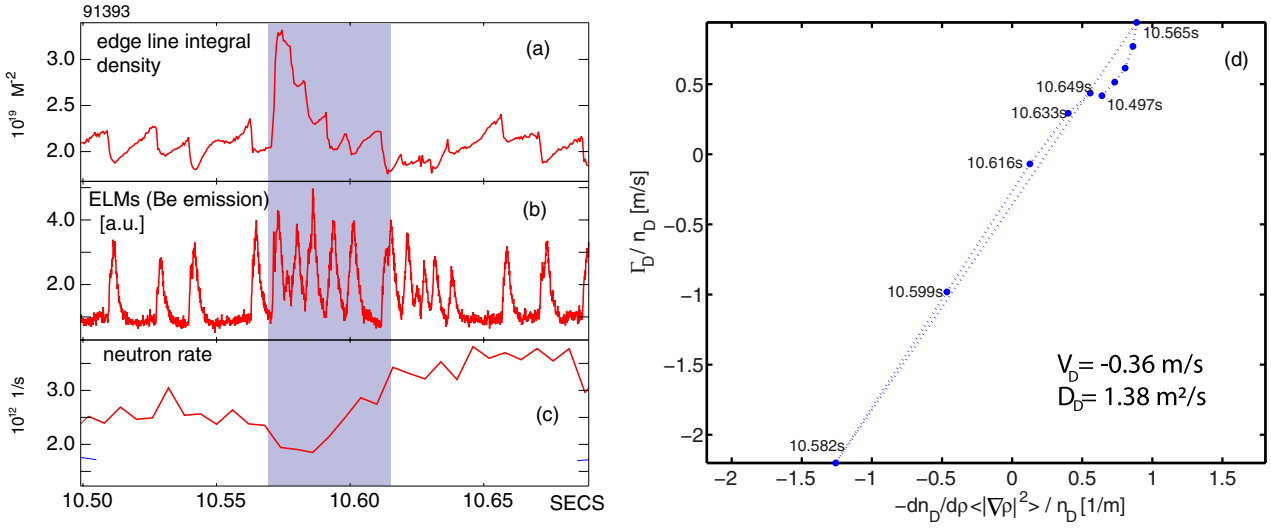

Figure 4. Detail of transients around the fourth pellet: (*a*) edge line integral density, (*b*) ELM signals, (*c*) neutron rate. The shaded area in panels (*a*)–(*c*) approximately represents the interval with an inverted density gradient. (*d*) Plot of the normalized particle flux Γ_D/n_D versus the normalized density gradient $dn_D/dr/n_D$ at $r/a = 0.5$. Corresponding time labels are shown.

still small, one possible explanation for this discrepancy could be the assumption that the plasma removed by ELMs in the mixed isotope case has the same isotope mix ratio as the measured time-averaged values given above for different diagnostics. However, during the post-pellet phase, when most of the losses occur, the lost plasma could have an isotope ratio closer to that of the pellet (deuterium in our case), which in turn will result in a smaller first coefficient in equation (1). This similarity in pellet fuelling throughput in different experiments points towards the same pellet particle loss mechanism, namely the dominant role of ELMs. Indeed, looking closely at the post-pellet line-integrated density signal (figure 4(*a*)) it is clear that the particles are lost in discrete events coinciding with ELMs. It takes about five ELMs to remove material deposited by a single pellet. This ratio is about the same as expected on ITER where the ELMs/pellet frequency ratio is expected to be about 40 Hz/10 Hz. Nevertheless the relative pellet size, and consequently the ELM size, is larger than that permitted on ITER. This is even true for a burst of high-frequency ELMs which immediately follow the pellet, as seen in figure 4. For those ELMs the normalized inverse frequency is $1/(f_{\mathrm{ELMs}}\tau_{\mathrm{E}}) = 1/(133\,\mathrm{Hz} \times 0.13\ \mathrm{s}) = 5.7\%$, that is about 10 times larger than the value required in ITER. Here $\delta W_{\mathrm{ELM}}/W_{\mathrm{tot}} \sim 1/(f_{\mathrm{ELMs}}\tau_{\mathrm{E}})$ is the size of an ELM that would carry all the energy transport losses. In summary the relation (1) is derived under the condition of an ITER like ratio of ELMs/pellet frequency, but the relative sizes of both pellets and ELMs are larger.

4.2. Core particle transport

When a pellet is injected into a plasma it creates a transient zone of reversed gradient of deuterium density. As a consequence, the deuterium ion particle flux reverses from outwards to inwards and consequently the deuterium concentration in the core increases, as manifest by an increase in the neutron rate signal in figure 4(*c*). This situation is transient. This is detailed in figure 4(*d*), where the simulated deuterium particle flux at $r/a = 0.5$ is plotted against the density gradient during one pellet cycle around the fourth pellet. The slope of this graph determines the deuterium particle diffusivity. When evaluated during the post-pellet phase lasting 70 ms the linear regression gives $D_{\mathrm{D}} = 1.38\ \mathrm{m^2\,s^{-1}}$. Note that this value comes from the Bohm-gyroBohm model with the C_{D} multiplier as described in section 3.3. In normalized units the deuterium diffusivity is $D_{\mathrm{D}}/\chi_{\mathrm{eff}} = 0.41$. Here $\chi_{\mathrm{eff}} = q/(n_{\mathrm{e}}\nabla T_{\mathrm{e}} + n_{\mathrm{i}}\nabla T_{\mathrm{i}}) = 3.3\ \mathrm{m^2\,s^{-1}}$ is the experimental effective single fluid heat diffusivity averaged over the pellet cycle and q is the total heat flux density. It has to be noted that pellets can also modify the temperature profile due to local cooling and this can change heat diffusivity itself. In our case the changes in heat diffusivity are within $\chi_{\mathrm{eff}} = 2.4$–$3.8\ \mathrm{m^2\,s^{-1}}$. Finally, it is interesting to see that the value of $D_{\mathrm{D}}/\chi_{\mathrm{eff}}$ is similar to those inferred from density peaking experiments in pure deuterium plasmas [24, 25].

As mentioned previously, neutron rate simulations could indicate that penetration of deuterium to the plasma core is faster at the beginning of the pellet train than during the later pellet fuelling phase. If enhancement of the neutron rate by a knock-on effect is insignificant then the value of $D_{\mathrm{D}}/\chi_{\mathrm{eff}}$ could be higher by a factor of up to about three during the first pellet, as seen in figure 3(*a*) from the low value of the simulated neutron rate during the first pellet, even for an elevated particle diffusion multiplier of $C_{\mathrm{D}} = 7$. One possible interpretation is that propagation of deuterium to the core depends on the isotope mix itself, or that transport properties of hydrogen and deuterium (e.g. their pinch velocities) are different from those in our transport model. This would link our data to the previous observations of enhanced particle diffusivity in the trace tritium experiment [26] and experiments with a variable H:D mix [5], although both were with gas fuelling. The main observation in these experiments is that the propagation

of ion isotope mixing could be anomalously fast. The gyro-kinetic simulations show that indeed in the ion temperature gradient regime the diffusivities for both ion species are higher than the electron diffusivity $D_H \sim D_D > D_e$ [4]. This could explain the fast propagation of isotope mixing from the edge to the core even with similar (but not equal) diffusivities for hydrogen isotopes. In other words our assumption of similar particle transport coefficients for the different isotopes does not contradict a possible 'isotope effect', whereby transport may be significantly modified when transitioning from a hydrogen-dominated to a deuterium-dominated plasma, or vice versa. For a given turbulence regime, set up by a given plasma composition, the difference in transport coefficients between the various isotopes is expected to be relatively small. The detailed gyro-kinetic modelling of core particle transport under our condition of isotope mixing by pellets is outside the scope of this paper. This work is now ongoing and will be subject of a separate paper [27].

5. Conclusion

We have demonstrated control of the hydrogen isotope mix in the plasma core when one isotope is delivered solely by shallow pellets from the edge. In our case we used deuterium pellets while neutral beams and gas fuelling used hydrogen. The isotope mix in the core was measured directly by CX spectroscopy. In addition, the isotope mix ratio was indirectly deduced from modelling using the JINTRAC code by matching the neutron rate and electron density including pellet transients. Both methods show that the H:D isotope mix in the core reached a ratio of 55%:45%, close to the target. The pellet particle flux required to reach such a mix ratio is $\Phi_{pel} = 0.045 P_{aux}/T_{e,ped}$. This value is in line with conventional shallow pellet fuelling experiments using deuterium pellets and deuterium plasma. Such similarity indicates that the pellet fuelling efficiency is governed by the same particle loss mechanism regardless of isotope mix, namely convective loss due to ELMs.

Deuterium is fuelled by edge pellets, and its particle transport is consistent with a simple model. Modelling also suggests that deuterium particle diffusivity could be higher at the beginning of the pellet train, when the plasma mainly consists of hydrogen, compared with the flat-top phase. For efficient burn control there is a demand for fast response of the isotope mix ratio to the source modifications. As shown here this could be of the order of the energy confinement time. Future work will concentrate on modelling the particle transport in the pellet cycle with more first-principles-based transport models.

Although the need for accuracy of isotope ratio control does not look very demanding it is important to understand all aspects of this control loop. In particular the question of isotope separation is important. It becomes clear that isotope control by pellet injectors with pure isotopes is very expensive and leads to a high tritium inventory with all its consequences for the environment. It is therefore important to build the physics basis for integrated pellet fuelling/isotope control to find the minimum isotope separation ratio which is still consistent with reliable burn control.

Acknowledgments

This work was carried out within the framework of the EUROfusion Consortium and received funding from the Euratom research and training programme 2014–2018 and 2018–2020 under grant agreement no. 633053 and from the RCUK Energy Programme grant no. EP/P012450/1. The views and opinions expressed herein do not necessarily reflect those of the European Commission. The authors would like to thank the anonymous referees for their valuable comments.

ORCID iDs

M. Valovič https://orcid.org/0000-0002-0855-1056
A. Boboc https://orcid.org/0000-0001-8841-3309
L. Frassinetti https://orcid.org/0000-0002-9546-4494
L. Garzotti https://orcid.org/0000-0002-3796-9814

References

[1] Estrada-Mila C., Candy J. and Waltz R.E. 2005 *Phys. Plasmas* **12** 022305
[2] Angioni C. *et al* 2018 *Phys. Plasmas* **25** 082517
[3] Mikkelsen D. *et al* 2015 *Phys. Plasmas* **22** 062301
[4] Bourdelle C. *et al* 2018 *Nucl. Fusion* **58** 076028
[5] Maslov M. *et al* 2018 *Nucl. Fusion* **58** 076022
[6] Maruyama S. *et al* 2012 *Proc. 24th Int. Conf. on Fusion Energy (San Diego, 2012)* p ITR/P5-24 (www-web.iaea.org/napc/physics/FEC/FEC2012/index.htm)
[7] Polevoi A. *et al* 2018 *Nucl. Fusion* **58** 056020
[8] Day C. and Giegerich T. 2013 *Fusion Eng. Des.* **88** 616
[9] Lang P. T. *et al* 2019 *Nucl. Fusion* **59** 026003
[10] Scott S. *et al* 1995 *Phys. Plasmas* **2** 2299
[11] Hawryluk R. *et al* 1994 *Phys. Rev. Lett.* **72** 3530
[12] Urano H. *et al* 2012 *Nucl. Fusion* **52** 114021
[13] Cordey J.G. *et al* 2000 *Plasma Phys. Control. Fusion* **42** A127
[14] Maggi C.F. *et al* 2018 *Plasma Phys. Control. Fusion* **60** 014045
[15] Romanelli M. *et al* (JET EFDA Contributors) 2014 JINTRAC: a system of codes for integrated simulation of tokamak scenarios *Plasma Fusion Res.* **9** 3403023
[16] Garzotti L. *et al* 2003 *Nucl. Fusion* **43** 1829
[17] Parail V. *et al* 2009 *Nucl. Fusion* **49** 075030
[18] Köchl F. *et al* 2018 *Plasma Phys. Control. Fusion* **60** 074008
[19] Pegourie B., Waller V., Nehme H., Garzotti L. and Geraud A. 2007 *Nucl. Fusion* **47** 44
[20] *TRANSP Code Version 18.2* (https://transp.pppl.gov) (https://doi.org/10.11578/dc.20180627.4)
[21] Kiptily V. 2018 private communication
[22] Valovič M. *et al* 2016 *Nucl. Fusion* **56** 066009
[23] Valovič M. *et al* 2018 *Plasma Phys. Control. Fusion* **60** 085013
[24] Garzotti L. *et al* 2006 *Nucl. Fusion* **46** 994
[25] Valovič M. *et al* 2004 *Plasma Phys. Control. Fusion* **46** 1877
[26] Zastrow K.-D. *et al* 2004 *Plasma Phys. Control. Fusion* **46** B255
[27] Marin M. 2019 private communication
[28] Joffrin E. *et al* 2019 *Nucl. Fusion* (https://doi.org/10.1088/1741-4326/ab2276)